ACS Macro Letters

pubs.acs.org/macroletters Letter

Can Polymer Helicity Affect Topological Chirality of Polymer Knots?

Yani Zhao, Jan Rothörl, Pol Besenius, Peter Virnau,* and Kostas Ch. Daoulas*

Cite This: ACS Macro Lett. 2023, 12, 234−240 Read Online

ACCESS | Metrics & More | Article Recommendations | Supporting Information

ABSTRACT: We investigate the effect of helicity in isolated polymers on the topological chirality of their knots with computer simulations. Polymers are described by generic worm-like chains (WLC), where helical conformations are promoted by chiral coupling between segments that are neighbors along the chain contour. The sign and magnitude of the coupling coefficient u determine the sense and strength of helicity. The corrugation of the helix is adjusted via the radius R of a spherical, hard excluded volume around each WLC segment. Open and compact helices are, respectively, obtained for R that is either zero or smaller than the length of the WLC bond, and R that is a few times larger than the bond length. We use a Monte Carlo algorithm to sample polymer conformations for different values of u, spanning the range from achiral polymers to chains with well-developed helices. Monitoring the average helix torsion and fluctuations of chiral order as a function of u, for two very different chain lengths, demonstrates that the coil−helix transition in this model is not a phase transition but a crossover. Statistical analysis of conformations forming the simplest chiral knots, 3_1, 5_1, and 5_2, demonstrates that topological mirror symmetry is broken—knots formed by helices with a given sense prefer one handedness over the other. For the 3_1 and 5_1 knots, positive helical sense favors positive handedness. Intriguingly, an opposite trend is observed for 5_2 knots, where positive helical sense promotes negative handedness. We argue that this special coupling between helicity and topological chirality stems from a generic mechanism: conformations where some of the knot crossings are found in "braids" formed by two tightly interwoven sections of the polymer.

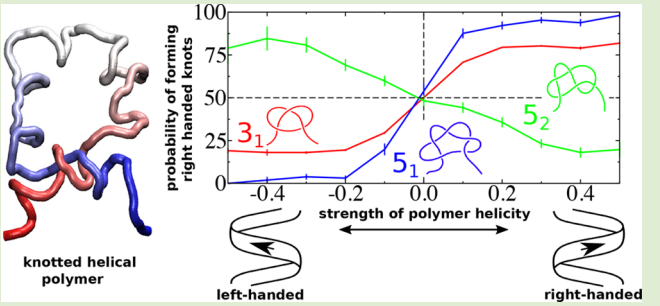

Molecular chirality can be classified into[1−3] geometrical, chemical, and topological chirality. Geometrical chirality applies to molecular objects that cannot[1−3] be superimposed with their mirror image by translation and/or rotation operations. Chemical chirality incorporates the influence of actual dynamics: a molecular configuration is chemically chiral when it cannot[3] be deformed into its mirror image by intramolecular transformations that are physically feasible under the given conditions, e.g., temperature. Topological chirality applies to molecular configurations that cannot[1−3] be transformed into their mirror image by a continuous deformation. Here, actual dynamics is irrelevant: bond lengths, valence angles, and dihedral angles can change arbitrarily, as long as the deformed molecule does not intersect itself.

Intriguingly, polymer chains form structures that are most natural to study topological chirality: knots. Figure 1a presents the simplest possible knot, the 3_1 (known as trefoil) knot, created, for illustration, on a generic bead−spring chain. Formally, knots are defined only in closed loops, but the concept is applicable to linear polymers after introducing an imaginary closure, indicated in Figure 1a by dashed lines. The closed 3_1 knot is topologically chiral because it cannot[1,4,5] be continuously transformed into its mirror image, Figure 1b. Generic cartoons in Figure 1c present the next two simplest 5_1 and 5_2 (known as fivefold) knots, that are chiral (we omit the achiral 4_1 knot). Since the closure is imaginary, knots evolve, disappear, and re-emerge, as linear polymers sample their conformational space.[6] For a polymer with chemically achiral conformations (such as the bead−spring polymer in Figure 1), one expects that knots and their mirror images are equally represented in the accessible conformational space. In other words, the mixture of knotted conformations is racemic. Conversely, the presence of chemical chirality might favor left- or right-handed knots, breaking the mirror symmetry of the knot mixture.

Although this hypothesis sounds reasonable, the actual knowledge on connections between chemical and topological chirality in polymers is very limited. Among others, the influence of chirality on interactions between knots[7] and their capability to meander through helical channels[8] have been studied, and recently, a 8_{19} knot with controlled handedness has been created artificially.[9] Many studies have investigated knotted structures in biopolymers such as proteins[10−15] and

Received: October 13, 2022
Accepted: January 23, 2023
Published: January 27, 2023

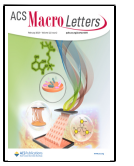

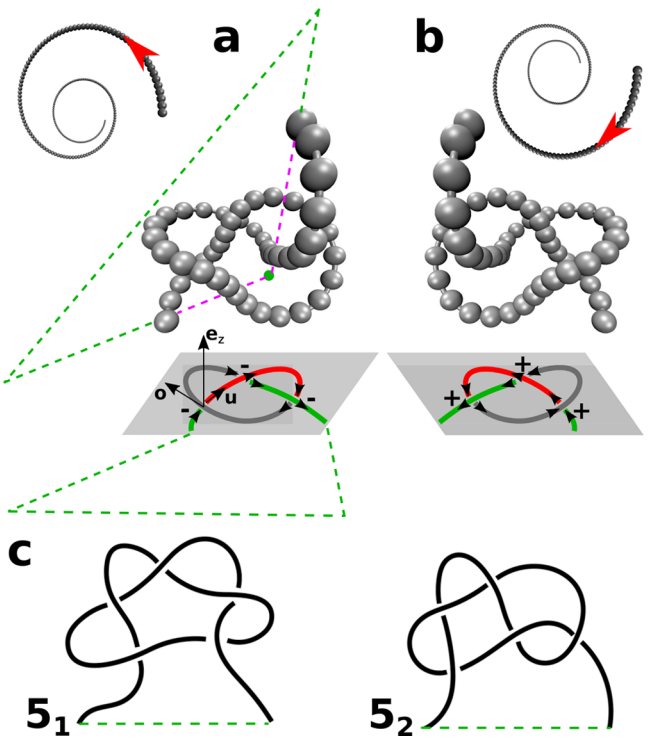

Figure 1. Panels (a) and (b) show, respectively, a conformation of an achiral bead−spring chain forming a left-handed 3_1 knot and its right-handed mirror image. Panel (a) explains the closure: two lines (green dashed lines) are determined by extrapolating to infinity two line segments (dashed purple lines), connecting the center-of-mass (green circle) of the conformation with the two ends of the chain. The closure is accomplished by connecting the two extrapolated lines far from the chain (green dashed line). The two-dimensional projection of the knots on the *xy*-plane (gray) is sketched below. Red, green, and gray mark the three arcs of each projected knot. The ± signs indicate the handedness of each crossing. Panel (a) illustrates the unit vectors along *z*-axis $\mathbf{e}_z$, overpassing bond **o**, and underpassing bond **u**, used to determine the handedness of one representative crossing. The insets of panels (a) and (b) explain, respectively, the definition of a left- and right-handed helix. They show a top view of a helix which rotates into the page along the direction of the red arrow. Panel (c) shows generic sketches of the next two simplest chiral knots, 5_1 and 5_2 (both examples show left-handed knots).

DNA.[16−22] While confining viral DNA in a capsid increases the knotting probability (≈95% for the 10 kilobase pairs (kbp) DNA strand of the P4 phage vir1 del22 tailless mutants[16,17]), knotting can be substantial even without confinement, provided that chains are long: a 166 kbp phage T4 GT7 DNA contains a knot in 70% of all cases.[21] Although biopolymers are a canonical example of chemically chiral macromolecules, research effort concentrated on detection and classification of knots, without correlating their topology with molecular-level features.[18] In particular, protein knots with both positive and negative handedness have been observed.[14,15] Intriguingly, chiral DNA knots have been constructed as early as 1995 by an enzymatic closure reaction using a left-handed Z-DNA to craft trefoils with positive handedness and right-handed B-DNA for trefoils with negative handedness.[23] However, because the knotted state was made permanent by the cyclic (closed) molecular architecture, the question regarding which knot handedness is thermodynamically favored by a right- or left-handed polymer chain was out of the scope of that study.

In this work, we consider a special, but very basic, example of chemical chirality: polymers that form right- or left-handed helices (Figure 1a and b explain the definition of a left- and right-handed helix). Our goal is to find generic relationships between helical sense and topological chirality of polymer knots.

We use a generic coarse-grained model to describe isolated helical polymer chains found in Θ solvent (ideal chains) and good solvent conditions. Polymers are represented by worm-like chains (WLC) with N segments (bonds). The interactions are defined through a Hamiltonian expressed in units of thermal energy k_BT as

$$\frac{H}{k_BT} = -\epsilon_b \sum_{i=1}^{N-1} \hat{\mathbf{t}}_i \cdot \hat{\mathbf{t}}_{i+1} + u \sum_{i=1}^{N-d} \sum_{j=i+1}^{i+d} \hat{\mathbf{r}}_{ij} \cdot [\hat{\mathbf{t}}_i \times \hat{\mathbf{t}}_j] + \sum_{i=1}^{N-[4R/b]} \sum_{j=i+[4R/b]}^{N} U(2R - |\mathbf{r}_{ij}|) \quad (1)$$

We arbitrarily choose one of the two directions along the contour of the WLC to number the segments. Accordingly, $\hat{\mathbf{t}}_i$ is a unit vector oriented along the i-th segment of the WLC and $\hat{\mathbf{r}}_{ij} = \mathbf{r}_{ij}/|\mathbf{r}_{ij}|$, where $\mathbf{r}_{ij}$ is the distance vector between the center-of-mass (COM) of the i-th and the j-th segment ($\mathbf{r}_{ij}$ is oriented from the i-th toward the j-th COM).

The first term in eq 1 manipulates polymer stiffness by adjusting the parameter ϵ_b. The length of the segments is fixed to b. The second term is a chiral potential that couples only those segments that are separated, along the WLC contour, by less than $d + 1$ segments and favors conformations with helical twist of prescribed sense. The magnitude of u controls the strength of the chiral coupling and its sign determines the helical sense. Namely, $u > 0$ and $u < 0$ result, respectively, in right-handed and left-handed helices, whereas $u = 0$ corresponds to an achiral polymer. Similar chiral interactions are used in studies of cholesteric phase,[24,25] chiral block copolymers,[26,27] simulations of chiral liquid crystals,[28] chiral aggregates,[29] coil−helix transitions,[30] and Go-like models of proteins.[31] The third term assigns to each segment a hard excluded volume with radius R, centered at its COM. Specifically, $U(2R - |\mathbf{r}_{ij}|) = +\infty$ when $2R - |\mathbf{r}_{ij}| \geq 0$ and $U(2R - |\mathbf{r}_{ij}|) = 0$ otherwise. There are no excluded volume interactions between segments that are separated by less than $[4R/b]$ segments along the WLC contour (angular brackets define the integer-part function). We sample the conformational space using a Monte Carlo (MC) reptation algorithm.[32] Details are provided in the Supporting Information.

Exploring the behavior of the generic model across the four-dimensional space of parameters ϵ_b, u, d, and R is outside the scope of this study. We choose three subsets of parameter space that are interesting for studying the behavior of knots. They have the same $\epsilon_b = 4$ and $d = 10$ but differ regarding the size of the excluded volume: R = 0, 0.5, and 2.5, respectively (R is given in units of b). u is a free parameter.

For $R = 0$ and 0.5 the chosen parameters lead to open helices where the pitch p is substantially larger[33] than the excluded volume of the segments, as illustrated in the main panel of Figure 2. This snapshot stems from MC simulations with $u = 0.5$. Studying knots in open helical polymers for both $R = 0$ and 0.5 is important because $R = 0.5$ retains some excluded volume. This situation might be more straightforward to realize in experiments (we provide further discussion later

https://doi.org/10.1021/acsmacrolett.2c00600
ACS Macro Lett. 2023, 12, 234−240

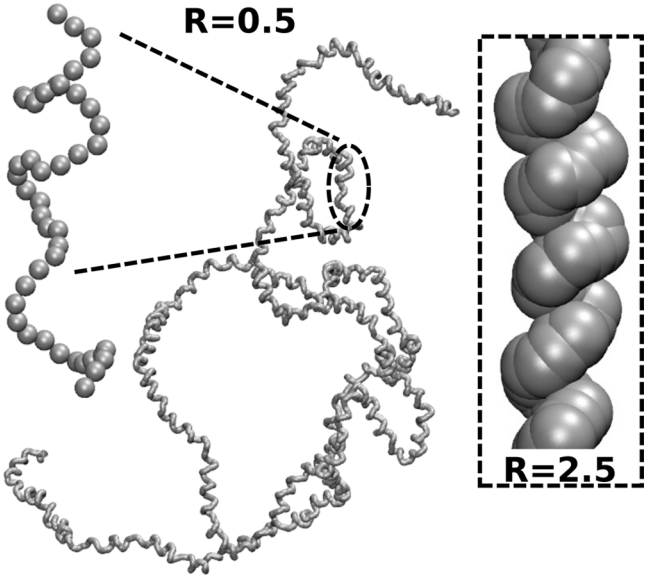

Figure 2. Main panel: Snapshot of an open WLC helix with $N = 2000$, $\epsilon_b = 4$, $d = 10$, and $u = 0.5$ obtained for small radius of excluded volume $R = 0.5$. The inset presents a section of a compact WLC helix obtained for the same N, ϵ_b, d, and u but with a large radius of excluded volume $R = 2.5$.

on). For $R = 2.5$, we obtain compact helices. The inset of Figure 2 presents a small part of a compact helix generated during MC simulations at $u = 0.5$.

Before exploring the behavior of knots, we must understand how helicity changes as a function of u. We quantify the helicity of chains using the ensemble-averaged torsion $\langle\tau\rangle$ of chains as an order parameter, defined as[34]

$$\langle\tau\rangle = \frac{1}{N-3}\left\langle \sum_{i=3}^{N-1} \frac{(r_i' \times r_i'')\cdot r_i'''}{|r_i' \times r_i''|^2} \right\rangle \tag{2}$$

Here r_i is the position vector of the i-th "monomer"; a WLC with N segments has $N + 1$ "monomers", i.e., $N - 1$ internal junctions and two ends. The derivatives are discretized[34] as $r_i' = \frac{1}{2}(r_{i+1} - r_{i-1})$, $r_i'' = r_{i+1} - 2r_i + r_{i-1}$, $r_i''' = \frac{1}{2}(r_{i+2} - 2(r_{i+1} - r_{i-1}) - r_{i-2})$. Figure 3a presents $\langle\tau\rangle$ as a function of u, for open, $R = 0$ and 0.5, and compact, $R = 2.5$, helices. For each R we present plots for two representative chain lengths, $N = 1000$ and 2000. Error bars are estimated from the standard error of the mean and are smaller than symbol size. Interestingly, $\langle\tau\rangle$ grows smoothly as u becomes larger, irrespective of R. Moreover, the plots of $\langle\tau\rangle$ for the two different chain lengths are, practically, on top of each other; that is, we do not observe finite system-size effects. These observations suggest that in our model the transition from achiral to chiral state is not a phase transition but a continuous crossover.[35] Formally, mirror symmetry is broken even for very small u, although in this limit chirality is weak.

One expects[36] that phase transition is absent when the breaking of mirror symmetry in isolated chains is caused by chiral intramolecular interactions between a limited number of consecutive monomers. In eq 1 the chiral potential couples d consecutive segments only. Such potentials resemble spin-couplings in Ising-like models of helical polymers.[37−42] They create equivalence[36,43] to an effective one-dimensional (1D) system with local interactions, which cannot exhibit a phase

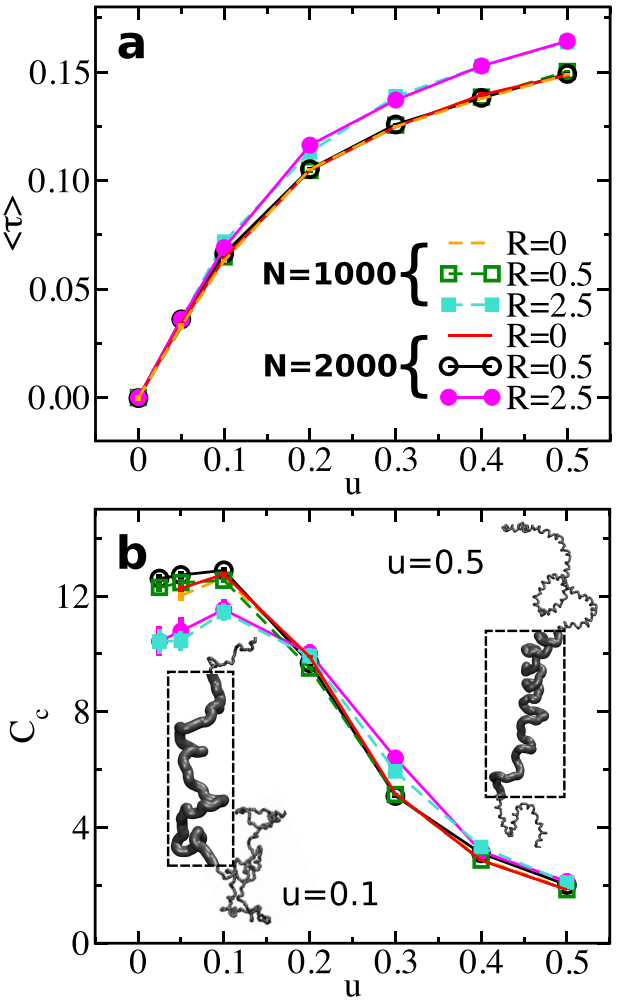

Figure 3. (a) Average torsion $\langle\tau\rangle$ shown as a function of u for chain lengths $N = 1000$ and 2000 (dashed and solid lines). For each N, data corresponding to $R = 0$, 0.5, and 2.5 are presented, as indicated by the legends. (b) Variance of chiral energy C_c (normalized by u) presented for polymers from panel (a) as a function of u. The color code is the same as in panel (a). The insets show snapshots of a WLC with $N = 1000$, at $u = 0.1$ (left) and 0.5 (right). To visualize the helical structure more clearly, parts of the polymer are shown enlarged in the dashed frames.

transition.[44] Some studies[35,45] have emphasized that explaining the phenomenology of mirror-symmetry breaking in single polymers through the thermodynamics of 1D systems might be an oversimplification because, typically, there are long-range interactions between repeat units. In principle, the excluded volume interaction in eq 1 correlates segments that are far apart along the WLC contour.[46] However, the trends in Figure 3a suggest that these correlations are not sufficient to cause a phase transition in our case.

We quantify the strength of fluctuations in chiral order through the variance of chiral energy, a heat capacity-like property, normalized by u:

$$C_c = \frac{1}{N}[\langle E_c^2\rangle - \langle E_c\rangle^2], \qquad E_c = \sum_{i=1}^{N-d}\sum_{j=i+1}^{i+d} \hat{\mathbf{r}}_{ij}\cdot[\hat{\mathbf{t}}_i \times \hat{\mathbf{t}}_j] \tag{3}$$

Figure 3b presents C_c calculated for the same systems as in Figure 3a. Error bars are again small; we estimate them from

https://doi.org/10.1021/acsmacrolett.2c00600
ACS Macro Lett. 2023, 12, 234−240

the expression of the standard error of the mean for variances ("fluctuation averages").[47] Figure 3b demonstrates that the fluctuations in chirality are stronger for small u. C_c exhibits a peak near $u = 0.1$, which is, however, weak. Importantly, the magnitude of the peak and the overall shape of C_c do not depend on N (the plots for $N = 1000$ and 2000 are practically on top of each other). This phenomenology of C_c is consistent with an absence of a phase transition. Visual inspection reveals that the stronger fluctuations at low u are associated with more "fluffy" conformations, exhibiting weakly helical and molten nonhelical regions. In contrast, helices are well formed for large u and dominate chain conformations. Figure 3b presents two snapshots of a chain with $N = 1000$ and $R = 0.5$, taken at $u = 0.1$ and 0.5.

We can now analyze knots. Generally, one can define the handedness of a knot by considering the minimal projection of the knot onto a plane.[48] Then, the handedness of a single crossing is defined as $h = \mathbf{e}_z \cdot ([\mathbf{o} \times \mathbf{u}])/|[\mathbf{o} \times \mathbf{u}]|$, where $\mathbf{e}_z$, $\mathbf{o}$, and $\mathbf{u}$ are, respectively, the unit vector along the z-axis, overpassing bond (at the projected crossing), and underpassing bond. The sign of the sum of all h in a minimal projection determines the handedness of the knot.[48,49] For example, the minimal projection of a trefoil has only three essential crossings (see Figure 1). The sum of h is positive for right-handed and negative for left-handed knots.

In practice, we calculate HOMFLYPT polynomials.[50,51] First, chain conformations, generated by MC, are "closed" by using the closure[49] explained in Figure 1. This closure enables calculations of HOMFLYPT polynomials with the Topoly package[52] to determine knot type and handedness.

Figure 4a presents the probability P_k (black lines) to find a knotted conformation in a $N = 2000$ chain, as a function of u for $R = 0$ (main panel), 0.5 (left inset), and 2.5 (right inset). The plots demonstrate that P_k is very small for chains with an excluded volume and highlight the difficulties in collecting data for analyzing knot handedness in this case. For $R = 0$ and 0.5, the P_k has a clear maximum at $u = 0$, whereas for $R = 2.5$, the plot (despite the large error bars) suggests a nonmonotonous dependence, i.e., P_k has a maximum at $u \neq 0$. Increasing u makes the chains stiffer, so both trends in Figure 4a are consistent with dependencies of P_k on chain stiffness that have been reported for achiral ideal[53] (monotonous decay) and achiral self-avoiding[54,55] (nonmonotonous decay) chains. In Figure 4a, for $R = 0$, we separately show the probability of observing a 3_1 (red line) knot, which is by far the most common knot type at this length scale. For $R = 0.5$ and 2.5, the preponderance of 3_1 knots is even stronger.

Figure 4b displays the probability $P_{k,norm}$ of observing 4_1 (orange line), 5_1 (blue line), and 5_2 (green line) knots, normalized by the total knotting probability. We use this normalization to emphasize the fraction of individual knots. The share of torus knots 3_1 (not shown here) and 5_1 increases with increasing $|u|$, while the portion of nontorus knots such as 4_1 or 5_2 is approximately constant for small $|u|$ and decreases for larger $|u|$. This trend resembles results obtained for DNA confined to bacteriophage capsids[16,17] and simulations describing such systems.[18,19]

Figure 4c is central for our work. It presents the probability P_{rk} that 3_1, 5_1, and 5_2 knots, when formed at given u, are right-handed. For 3_1 knots (red line), the mirror symmetry is clearly broken for all three R considered in our study, because there is an excess and depletion of right-handed knots for $u > 0$ and $u < 0$, respectively. However, there is a qualitative difference

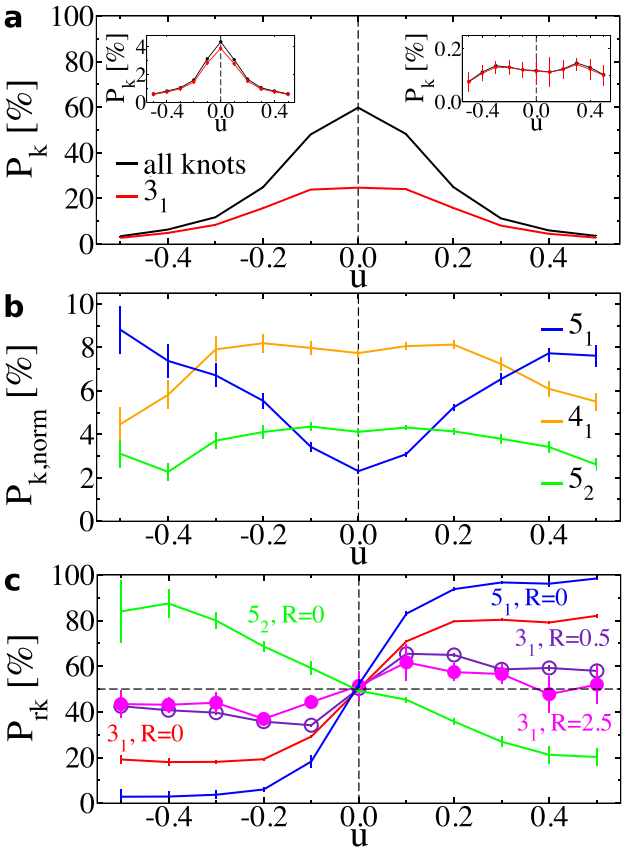

Figure 4. (a) The main panel shows the total knotting and occurrence probability, both indicated by P_k, of 3_1 knots as a function of u, for chains with $R = 0$ and $N = 2000$. Error bars are smaller than the width of the line. The left and right insets show the total knotting and occurrence probability for 3_1 knots for $R = 0.5$ and 2.5, respectively. (b) Occurrence probability $P_{k,norm}$ of 4_1, 5_1, and 5_2 knots for chains with $R = 0$ and $N = 2000$ normalized by the total knotting probability. (c) Probability P_{rk} that a knot formed at given u is right handed. $P_{rk} = 50\%$ (horizontal black dashed line) indicates no preferred handedness. Data for 3_1 knots obtained with $R = 0$, 0.5, and 2.5, and for fivefold knots obtained with $R = 0$ are presented, as indicated near each plot.

regarding how P_{rk} changes as a function of u for chains without and with excluded volume. Overall, we observe that for R = 0 the effect of helicity on handedness of knots is much stronger than for $R > 0$, that is, deviations from $P_{rk} = 50\%$ are more pronounced. Furthermore, P_{rk} increases monotonously for $R = 0$ to saturate (at least for the considered range of u) to a constant value. In contrast, for chains with excluded volume, the effect of helicity on knots is stronger for small u. Specifically, P_{rk} exhibits a peak near $u = 0.1$ and decays after that. Importantly, for the largest excluded volume $R = 2.5$, the excess (depletion) of right-handed knots is smaller than for $R = 0.5$.

P_{rk} shows broken mirror symmetry also for 5_1 and 5_2 knots. Because it is challenging to accumulate reliable statistics on 5_1 and 5_2 knots for chains with an excluded volume (see insets in Figure 4a), Figure 4c presents results only for $R = 0$. The dependence of P_{rk} on u for 5_1 knots (blue line) qualitatively reproduces the trends observed for 3_1 knots: we see pronounced excess (depletion) of right-handed knots for $u > 0$ ($u < 0$), which saturates at high u. This behavior is consistent with 5_1 knot being a torus knot which (for open chains) can be obtained from a 3_1 knot by one extra winding around the knot

https://doi.org/10.1021/acsmacrolett.2c00600
ACS Macro Lett. 2023, 12, 234−240

contour. Intriguingly, however, 5_2 knots (green line) show an opposite trend; there is a surplus of right-handed knots for $u < 0$ and a depletion for $u > 0$. This, at first glance, unexpected behavior of 5_2 knots demonstrates that the handedness of knots may not coincide with the helical sense of the molecule.

We suggest that the coupling between helicity and topological chirality found in our simulations stems (to large extent, at least) from a generic mechanism. Namely, it is caused by conformations where some of the knot crossings are encapsulated in a "braid" formed by two interwoven helical subchains. Figure 5a illustrates three representative conformations of 3_1, 5_1, and 5_2 knots with such a braid (the braided part is enlarged, in a separate frame) for $R = 0$ (for clarity, we are showing only the knotted part of an $N = 2000$ chain). The sense (direction) of winding of the subchains around each other is the same as the sense of the polymer helix (positive in the examples of Figure 5a).

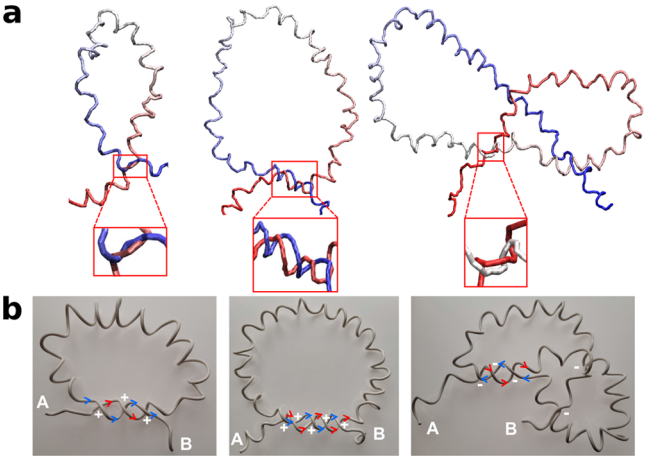

Figure 5. (a) Snapshots of parts of an $N = 2000$ chain forming 3_1, 5_1, and 5_2 knots (from left to right) for $u = 0.5$ and $R = 0$, illustrating typical shapes of knots with braids (for these parameters). The braided part of the knots is shown enlarged, in a separate frame. (b) Illustrations of the same knots based on an idealized physical (wire) model. The chain contour is traced from end A toward end B. Red and blue arrows, respectively, mark the direction of motion along the first and the second polymer strand forming the braid. The topology of 3_1 and 5_1 knots is such that the two strands are traveled in the same direction, whereas for the 5_2 knot, they are traveled in opposite directions. This difference affects the handedness of the crossings, which is indicated by the ± signs.

Initially, our explanation is motivated by visual inspection of knotted conformations. Of course, visual analysis cannot be systematic because of the significant amount of knotted conformations and their variability. However, there are also several more quantitative arguments that favor our conjecture based on indirect evidence. First of all, helices, say, with positive helical sense, interwoven into a braid with positive twist can *simultaneously* explain the preference for *positive* handedness in 3_1 and 5_1 and the *negative* handedness in 5_2 knots, respectively. Figure 5b provides explanatory illustrations based on an idealized physical (wire) model of helical knotted chains. These illustrations may also indicate that for large $|u|$ torus knots, 3_1 and 5_1 are easier to form and have a simpler braiding pattern than, for example, a 5_2 knot, providing an interpretation for results observed in Figure 4b. A similar analysis of knots in terms of "braids" was performed[56,57] to explain the occurrence of certain knot types in template synthesis of molecular knots.[58] Second, we take into account that in interwoven helices segments come close to each other. Therefore, for $R = 0$, we eliminate from the sample knotted conformations where at least two segments (separated by more than d segments along the WLC contour) are found closer than a cutoff distance r_{min}; a typical choice is $r_{min} = 1.5$. For knots that survive this screening (and therefore have no tightly packed braids), the deviations of P_{rk} from 50% are significantly reduced. Plots are available in the Supporting Information. Consistent with the effect of screening for $R = 0$, we observe a reduced deviation of P_{rk} from 50% in systems with excluded volume, especially $R = 2.5$ (Figure 4c). In the latter case, compact helices do not allow for molecular interdigitation sufficient for forming braids. Finally, we note that for $R = 0.5$ and 2.5 there is also a similarity between the nonmonotonous dependence of P_{rk} on u and the behavior of C_c in Figure 3b. This observation suggests that strong fluctuations in local chain conformations and helicity promote interdigitation.

Various studies[59−63] have revealed that special packing of molecules with helical surface affects mesoscopic chiral order in multichain systems. In this respect, our observations regarding the relationship between local packing of helices and topological chirality of knots are not surprising. Still, it is rather unexpected that the fraction of conformations found in this particular knotted state is sufficiently large to cause perceptible mirror-symmetry breaking for the entire set of 3_1, 5_1, and 5_2 knots. Detailed analysis of knot handedness versus the amount of monomers contained in a knot demonstrates that broken mirror symmetry is more pronounced for smaller knots. Hence, it is plausible to expect that the effects of helicity on topological chirality of the entire population of knots in longer chains (than those that have been considered here) will be reduced.

Our findings are based on a generic molecular model but can be extrapolated to actual helical polymers. We expect that an excess of knots with one sense of handedness might be observed in chiral polymers where helices have well-separated "ridges" and "valleys", the analog of open helices formed in our model at a small excluded volume. Polyisocyanates[64,65] might be one example, taking into account that the formation of their lyotropic cholesteric phases can be explained[62] assuming a strongly corrugated, screw-like, helical molecular surface. Another candidate are biopolymers with polyproline helices of type PP-II. In contrast, we do not expect strong preferred handedness for knots in polymers with compact helices. Here, representative examples are biopolymers with polyproline helices of type PP-I or α-helices.[66] The topology of single knotted polymer conformations can be analyzed by modern imaging techniques such AFM.[67]

■ ASSOCIATED CONTENT

Supporting Information

The Supporting Information is available free of charge at https://pubs.acs.org/doi/10.1021/acsmacrolett.2c00600.

Details on the applied reptation algorithm; The effect of exclusion of conformations with closely packed segments on handedness of trefoil knots; The effect of polymer helicity on the prevalent type of fivefold knots (PDF)

https://doi.org/10.1021/acsmacrolett.2c00600
ACS Macro Lett. 2023, 12, 234−240

AUTHOR INFORMATION

Corresponding Authors

Peter Virnau − *Department of Physics, Johannes Gutenberg University Mainz, 55128 Mainz, Germany*; Email: virnau@uni-mainz.de

Kostas Ch. Daoulas − *Max Planck Institute for Polymer Research, 55128 Mainz, Germany*; orcid.org/0000-0001-9278-6036; Phone: +49 (0)6131 379218; Email: daoulas@mpip-mainz.mpg.de

Authors

Yani Zhao − *Max Planck Institute for Polymer Research, 55128 Mainz, Germany*; orcid.org/0000-0003-1430-4518

Jan Rothörl − *Department of Physics, Johannes Gutenberg University Mainz, 55128 Mainz, Germany*

Pol Besenius − *Department of Chemistry, Johannes Gutenberg University Mainz, 55128 Mainz, Germany*; orcid.org/0000-0001-7478-4459

Complete contact information is available at: https://pubs.acs.org/10.1021/acsmacrolett.2c00600

Funding

Open access funded by Max Planck Society.

Notes

The authors declare no competing financial interest.

ACKNOWLEDGMENTS

We are grateful to Kurt Kremer for helpful discussions related to this work and useful comments made after reading our manuscript. We thank Wanda Niemyska and Pawel Rubach for helping us with using the Topoly software for knot analysis. P.V. and K.C.D. acknowledge funding from the Deutsche Forschungsgemeinschaft (DFG, German Research Foundation): Project Number 233630050 - TRR 146.

REFERENCES

(1) Mislow, K. A Commentary on the Topological Chirality and Achirality of Molecules. *Croat. Chem. Acta* **1996**, *69*, 485−511.

(2) Chambron, J. C.; Dietrich-Buchecker, C.; Sauvage, J. P. From Classical Chirality to Topologically Chiral Catenands and Knots. *Top. Curr. Chem.* **1993**, *165*, 131−162.

(3) Bonchev, D.; Rouvray, D. H. *Chemical Topology: Applications and Techniques*; Gordon and Breach Science Publishers: Amsterdam, 2000.

(4) Dehn, M. Die beiden Kleeblattschlingen. *Math. Ann.* **1914**, *75*, 402−413.

(5) Fielden, S. D.; Leigh, D. A.; Woltering, S. L. Molecular Knots. *Angew. Chem., Int. Ed.* **2017**, *56*, 11166−11194.

(6) Tubiana, L.; Rosa, A.; Fragiacomo, F.; Micheletti, C. Spontaneous Knotting and Unknotting of Flexible Linear Polymers: Equilibrium and Kinetic Aspects. *Macromolecules* **2013**, *46*, 3669−3678.

(7) Najafi, S.; Tubiana, L.; Podgornik, R.; Potestio, R. Chirality Modifies the Interaction between Knots. *EPL* **2016**, *114*, 50007.

(8) Ruskova, R.; Racko, D. Channels with Helical Modulation Display Stereospecific Sensitivity for Chiral Superstructures. *Polymers* **2021**, *13*, 3726.

(9) Carpenter, J. P.; McTernan, C. T.; Greenfield, J. L.; Lavendomme, R.; Ronson, T. K.; Nitschke, J. R. Controlling the Shape and Chirality of an Eight-Crossing Molecular Knot. *Chem.* **2021**, *7*, 1534−1543.

(10) Taylor, W. A. Deeply Knotted Protein Structure and How it Might Fold. *Nature* **2000**, *406*, 916−919.

(11) Virnau, P.; Mirny, L. A.; Kardar, M. Intricate Knots in Proteins: Function and Evolution. *PLoS Comput. Biol.* **2006**, *2*, No. e122.

(12) Lua, R. C.; Grosberg, A. Y. Statistics of Knots, Geometry of Conformations, and Evolution of Proteins. *PLoS Comp. Biol.* **2006**, *2*, 350−357.

(13) Boelinger, D.; Sulkowska, J.; Hsu, H.-P.; Mirny, L.; Kardar, M.; Onuchic, J.; Virnau, P. A Stevedore's Protein Knot. *PLOS Comp. Biol.* **2010**, *6*, e1000731.

(14) Virnau, P.; Mallam, A.; Jackson, S. Structures and Folding Pathways of Topologically Knotted Proteins. *J. Phys: Cond. Matt.* **2011**, *23*, 033101.

(15) Jarmolinska, A. I.; Perlinska, A. P.; Runkel, R.; Trefz, B.; Ginn, H. M.; Virnau, P.; Sulkowska, J. I. Proteins' Knotty Problems. *J. Mol. Biol.* **2019**, *431*, 244−257.

(16) Arsuaga, J.; Vazquez, M.; Trigueros, S.; Sumners, D. W.; Roca, J. Knotting Probability of DNA Molecules Confined in Restricted Volumes: DNA Knotting in Phage Capsids. *Proc. Natl. Acad. Sci. U.S.A.* **2002**, *99*, 5373−5377.

(17) Arsuaga, J.; Vazquez, M.; McGuirk, P.; Trigueros, S.; Sumners, D. W.; Roca, J. DNA Knots Reveal a Chiral Organization of DNA in Phage Capsids. *Proc. Natl. Acad. Sci. U.S.A.* **2005**, *102*, 9165−9169.

(18) Marenduzzo, D.; Orlandini, E.; Stasiak, A.; Sumners, D. W.; Tubiana, L.; Micheletti, C. DNA−DNA Interactions in Bacteriophage Capsids are Responsible for the Observed DNA Knotting. *Proc. Natl. Acad. Sci. U.S.A.* **2009**, *106*, 22269−22274.

(19) Reith, D.; Cifra, P.; Stasiak, A.; Virnau, P. Effective Stiffening of DNA due to Nematic Ordering Causes DNA Molecules Packed in Phage Capsids to Preferentially Form Torus Knots. *Nucleic Acids Res.* **2012**, *40*, 5129−5137.

(20) Rieger, F. C.; Virnau, P. A Monte Carlo Study of Knots in Long Double-Stranded DNA Chains. *PLoS Comp. Biol.* **2016**, *12*, e1005029.

(21) Plesa, C.; Verschueren, D.; Pud, S.; van der Torre, J.; Ruitenberg, J. W.; Witteveen, M. J.; Jonsson, M. P.; Grosberg, A. Y.; Rabin, Y.; Dekker, C. Direct Observation of DNA Knots using a Solid-State Nanopore. *Nat. Nanotechnol.* **2016**, *11*, 1093−1097.

(22) Kumar Sharma, R.; Agrawal, I.; Dai, L.; Doyle, P. S.; Garaj, S. Complex DNA Knots Detected with a Nanopore Sensor. *Nat. Commun.* **2019**, *10*, 4473.

(23) Du, S.; Stollar, B.; Seeman, N. A Synthetic DNA Molecule in 3 Knotted Topologies. *J. Am. Chem. Soc.* **1995**, *117*, 1194−1200.

(24) van der Meer, B.; Vertogen, G.; Dekker, A. J.; Ypma, J. G. J. A Molecular-Statistical Theory of the Temperature-Dependent Pitch in Cholesteric Liquid Crystals. *J. Chem. Phys.* **1976**, *65*, 3935−3943.

(25) Osipov, M. In *Liquid Crystalline and Mesomorphic Polymers*; Shibaev, V. P., Lam, L., Eds.; Springer, 1994; pp 1−25.

(26) Zhao, W.; Russell, T. P.; Grason, G. M. Chirality in Block Copolymer Melts: Mesoscopic Helicity from Intersegment Twist. *Phys. Rev. Lett.* **2013**, *110*, 058301.

(27) Grason, G. M. Chirality Transfer in Block Copolymer Melts: Emerging Concepts. *ACS Macro Lett.* **2015**, *4*, 526−532.

(28) Memmer, R.; Kuball, H.-G.; Schönhofer, A. Computer Simulation of Chiral Liquid Crystal Phases I. The Polymorphism of the Chiral Gay-Berne Fluid. *Liq. Cryst.* **1993**, *15*, 345−360.

(29) Sutherland, B. J.; Olesen, S. W.; Kusumaatmaja, H.; Morgan, J. W. R.; Wales, D. J. Morphological Analysis of Chiral Rod Clusters from a Coarse-Grained Single-Site Chiral Potential. *Soft Matter* **2019**, *15*, 8147−8155.

(30) Kemp, J.; Chen, Z. Formation of Helical States in Wormlike Polymer Chains. *Phys. Rev. Lett.* **1998**, *81*, 3880−3883.

(31) Wołek, K.; Gómez-Sicilia, Á.; Cieplak, M. Determination of Contact Maps in Proteins: a Combination of Structural and Chemical Approaches. *J. Chem. Phys.* **2015**, *143*, 243105.

(32) Wall, F.; Mandel, F. Macromolecular Dimensions Obtained by an Efficient Monte Carlo Method without Sample Attrition. *J. Chem. Phys.* **1975**, *63*, 4592−4595.

(33) Glagolev, M. K.; Vasilevskaya, V. V.; Khokhlov, A. R. Compactization of Rigid-Chain Amphiphilic Macromolecules with Local Helical Structure. *Polymer Science, Ser. A* **2010**, *52*, 761−774.

(34) Magee, J. E.; Song, Z.; Curtis, R. A.; Lue, L. Structure and Aggregation of a Helix-Forming Polymer. *J. Chem. Phys.* **2007**, *126*, 144911.
(35) Boehm, C. R.; Terentjev, E. M. Minimal Model of Intrinsic Chirality to Study the Folding Behavior of Helical Polymers. *Macromolecules* **2014**, *47*, 6086−6094.
(36) Grosberg, A. Y.; Khokhlov, A. R. *Statistical Physics of Macromolecules*; AIP Press: New York, 1994.
(37) Selinger, J. V.; Selinger, R. L. B. Theory of Chiral Order in random Copolymers. *Phys. Rev. Lett.* **1996**, *76*, 58−61.
(38) Green, M. M.; Park, J.-W.; Sato, T.; Teramoto, A.; Lifson, S.; Selinger, R. L. B.; Selinger, J. V. The Macromolecular Route to Chiral Amplification. *Angew. Chem., Int. Ed.* **1999**, *38*, 3138−3154.
(39) van Gestel, J.; van der Schoot, P.; Michels, M. A. J. Amplification of Chirality in Helical Supramolecular Polymers Beyond the Long-Chain Limit. *J. Chem. Phys.* **2004**, *120*, 8253−8261.
(40) van Gestel, J. Amplification of Chirality in Helical Supramolecular Polymers: The Majority-Rules Principle. *Macromolecules* **2004**, *37*, 3894−3898.
(41) Jouvelet, B.; Isare, B.; Bouteiller, L.; van der Schoot, P. Direct Probing of the Free-Energy Penalty for Helix Reversals and Chiral Mismatches in Chiral Supramolecular Polymers. *Langmuir* **2014**, *30*, 4570−4575.
(42) van Gestel, J.; Palmans, A. R. A.; Titulaer, B.; Vekemans, J. A. J. M.; Meijer, E. W. "Majority-Rules" Operative in Chiral Columnar Stacks of C3-Symmetrical Molecules. *J. Am. Chem. Soc.* **2005**, *127*, 5490−5494.
(43) Zimm, B. H.; Bragg, J. K. Theory of the Phase Transition between Helix and Random Coil in Polypeptide Chains. *J. Chem. Phys.* **1959**, *31*, 526−535.
(44) Landau, L. D.; Lifshitz, E. M. *Statistical Physics*; Pergamon: London, 1959; Vol. 5.
(45) Hansmann, U. H.; Okamoto, Y. Finite-Size Scaling of Helix-Coil Transitions in Poly-Alanine Studied by Multicanonical Simulations. *J. Chem. Phys.* **1999**, *110*, 1267−1276.
(46) Doi, M.; Edwards, S. F. *The Theory of Polymer Dynamics*; Claredon Press: Oxford, England, 1986.
(47) Allen, M. P.; Tildesley, D. J. *Computer Simulation of Liquids*; Clarendon Press: Oxford, 1989.
(48) Livingston, C. *Knot Theory*; Mathematical Association of America: WA, 1993.
(49) Virnau, P. Detection and Visualization of Physical Knots in Macromolecules. *Phys. Procedia* **2010**, *6*, 117−125.
(50) Freyd, P.; Yetter, D.; Hoste, J.; Lickorish, W. B. R.; Millett, K.; Ocneanu, A. A New Polynomial Invariant of Knots and Links. *Bull. Am. Math. Soc.* **1985**, *12*, 239−246.
(51) Przytycki, J.; Traczyk, P. Invariants of Links of Conway Type. *Kobe J. Math* **1987**, *4*, 115−139.
(52) Dabrowski-Tumanski, P.; Rubach, P.; Niemyska, W.; Gren, B. A.; Sulkowska, J. I. Topoly: Python package to analyze topology of polymers. *Briefings in Bioinformatics* **2021**, *22*, bbaa196.
(53) Virnau, P.; Rieger, F. C.; Reith, D. Influence of Chain Stiffness on Knottedness in Single Polymers. *Biochem. Soc. Trans.* **2013**, *41*, 528−532.
(54) Coronel, L.; Orlandini, E.; Micheletti, C. Non-Monotonic Knotting Probability and Knot Length of Semiflexible Rings: the Competing Roles of Entropy and Bending Energy. *Soft Matter* **2017**, *13*, 4260−4267.
(55) Uehara, E.; Coronel, L.; Micheletti, C.; Deguchi, T. Bimodality in the Knotting Probability of Semiflexible Rings Suggested by Mapping with Self-Avoiding Polygons. *React. Funct. Polym.* **2019**, *134*, 141−149.
(56) Polles, G.; Marenduzzo, D.; Orlandini, E.; Micheletti, C. Self-assembling knots of controlled topology by designing the geometry of patchy templates. *Nat. Commun.* **2015**, *6*, 6423.
(57) Marenda, M.; Orlandini, E.; Micheletti, C. Discovering privileged topologies of molecular knots with self-assembling models. *Nat. Commun.* **2018**, *9*, 3051.
(58) Ayme, J.-F.; Beves, J. E.; Campbell, C. J.; Leigh, D. A. Template synthesis of molecular knots. *Chem. Soc. Rev.* **2013**, *42*, 1700−1712.
(59) Ferrarini, A.; Moro, G.; Nordio, P. Shape Model for Ordering Properties of Molecular Dopants Inducing Chiral Mesophases. *Mol. Phys.* **1996**, *87*, 485−499.
(60) De Michele, C.; Zanchetta, G.; Bellini, T.; Frezza, E.; Ferrarini, A. Hierarchical Propagation of Chirality through Reversible Polymerization: The Cholesteric Phase of DNA Oligomers. *ACS Macro Lett.* **2016**, *5*, 208−212.
(61) Straley, J. Theory of Piezoelectricity in Nematic Liquid Crystals, and of the Cholesteric Order. *Phys. Rev. A* **1976**, *14*, 1835−1841.
(62) Green, M. M.; Peterson, N. C.; Sato, T.; Teramoto, A.; Cook, R.; Lifson, S. A Helical Polymer with a Cooperative Response to Chiral Information. *Science* **1995**, *268*, 1860−1866.
(63) Earl, D. J.; Wilson, M. R. Predictions of Molecular Chirality and Helical Twisting Powers: A Theoretical Study. *J. Chem. Phys.* **2003**, *119*, 10280−10288.
(64) Green, M. M.; Reidy, M. P.; Johnson, R. D.; Darling, G.; O'Leary, D. J.; Willson, G. Macromolecular Stereochemistry: the Out-of-Proportion Influence of Optically Active Comonomers on the Conformational Characteristics of Polyisocyanates. The Sergeants and Soldiers Experiment. *J. Am. Chem. Soc.* **1989**, *111*, 6452.
(65) Sato, T.; Sato, Y.; Umemura, Y.; Teramoto, A.; Nagamura, Y.; Wagner, J.; Weng, D.; Okamoto, Y.; Hatada, K.; Green, M. M. Polyisocyanates and the Interplay of Experiment and Theory in the Formation of Lyotropic Cholesteric States. *Macromolecules* **1993**, *26*, 4551−4559.
(66) Pauling, L.; Corey, R. B.; Branson, H. R. The Structure of Proteins: two Hydrogen-Bonded Helical Configurations of the Polypeptide Chain. *Proc. Natl. Acad. Sci. U.S.A.* **1951**, *37*, 205−211.
(67) Schappacher, M.; Deffieux, A. Imaging of Catenated, Figure-of-Eight, and Trefoil Knot Polymer Rings. *Angew. Chem. Int. Ed.* **2009**, *48*, 5930−5933.

https://doi.org/10.1021/acsmacrolett.2c00600
ACS Macro Lett. 2023, 12, 234−240